RAA 2016 Vol. **16** No. **12**, 182 (7pp) doi: 10.1088/1674–4527/16/12/182
© 2016 National Astronomical Observatories, CAS and IOP Publishing Ltd.
http://www.raa-journal.org *http://iopscience.iop.org/raa*

Research in Astronomy and Astrophysics

Millimeter observations of organic molecules toward high-mass star formation region G34.26+0.15

Li Fu[1,2] and Guo-Man Lin[3]

[1] School of Chemistry & Material Science, Langfang Teachers University, Langfang, 065000, China; *fuli668@126.com*
[2] College of Chemistry & Molecular Engineering, Peking University, Beijing, 100871, China
[3] School of Physics & Electronics, Langfang Teachers University, Langfang, 065000, China

Received 2016 June 16; accepted 2016 August 2

Abstract To investigate the chemical origination of organic molecules CH_3OH, CH_3OCH_3, C_2H_5OH, CH_3OCH, CH_3CN, C_2H_3CN and C_2H_5CN in the hot core associated with high-mass star formation region G34.26+0.15, Submillimeter Array observations were made with its 230 GHz receiver. The molecular gas distribution has shown that the oxygen- and nitrogen-containing molecules peak at different positions. Comparing the spatial distributions with rotational temperatures and fractional abundances of the observed molecules, we discuss the possible chemical origination of these organic molecules.

Key words: astrochemistry — molecular processes — line: identification — ISM: abundances

1 INTRODUCTION

Ultracompact HII (UC HII) regions are thought to be indicators of high-mass star formation (Churchwell 2002). Hot molecular cores (HMCs) represent the immediate environments where massive stars were recently born. HMCs are observed to have compact structure, be dense, have a warm molecular gas component and are frequently found around high-mass star formation sites associated with UC HII regions (Kurtz et al. 2000). Their hot core phase also shows rich molecular line emissions at (sub)millimeter wavelengths. Therefore, observations of HMCs are crucial for characterizing physical and chemical structures associated with massive star formation. G34.26+0.15 is one of the well studied high-mass star formation regions, at a distance of 3.7 kpc from the Sun (Kuchar & Bania 1994). Molecular line observations suggested that massive star formation is taking place in this star formation complex (e.g., Liu et al. 2013). Three UC HII regions ("A, B and C") have been identified by continuum observations at centimeter wavelengths (Wood & Churchwell 1989; Avalos et al. 2006). Single dish observations of multiple organic molecular lines suggested that hot gas components are present in the G34.26+0.15 star formation complex (Hatchell et al. 1998; Fontani et al. 2007), while higher spatial resolution observations with interferometers showed that the hot gas components (which are HMCs) are associated with UC HII region "C" (Mookerjea et al. 2007). However, only a few molecular transitions of C_2H_5CN, CH_3OCH_3 and $HCOOCH_3$ were observed in previous observations with higher spatial resolution (Mookerjea et al. 2007). To obtain accurate physical parameters, many transitions of the same species spanning wide energy ranges are needed. In this paper, we present Submillimeter Array (SMA)[1] observations of multiple transitions in organic molecules. Using the multiple lines, we derive relatively accurate physical parameters and discuss the physical and chemical environments of the G34.26+0.15 HMC.

2 OBSERVATIONS

We obtained the data from the SMA data archive. The SMA observations of G34.26+0.15 were made in April 2011 using its compact array. The phase tracking center of the observations was R.A. (J2000) $= 18^{\rm h}53^{\rm m}18.573^{\rm s}$ and Dec. (J2000) $= 01°14'58.3''$. The double spectral sideband mode was used and centered at 227.5 GHz for the lower sideband and 239.5 GHz for the upper sideband. The spectral resolution was 0.8125 MHz, which corresponds to a velocity resolution of $\sim 1.1\,{\rm km\,s^{-1}}$. Quasi-stellar object (QSO) 3C 279 and Saturn were employed for bandpass calibration. QSOs 1911–201 and 1741–038 were observed for phase calibration. Absolute flux density was scaled by observing Saturn, and is estimated to be accurate to within 15%. Data reduction was done in Miriad. The resultant full width at half maximum beam size was $3.1'' \times 2.5''$ (PA $= -58°$). The 1σ rms of continuum and line emissions were 0.03 and 0.2 Jy beam^{-1}, respectively.

[1] The Submillimeter Array is a joint project between the Smithsonian Astrophysical Observatory and the Academia Sinica Institute of Astronomy and Astrophysics and is funded by the Smithsonian Institution and the Academia Sinica.

3 RESULTS

3.1 Continuum Image

The continuum image of G34.26+0.15 at 1.3 mm is shown in Figure 1. In this image, a compact source structure is revealed and the continuum peak at the 1.3 mm waveband is consistent with the UC HII region "C." Therefore the emission at 1.3 mm may contain free-free emission. Two dimensional Gaussian fitting to the continuum image gives the peak flux of 9.5 ± 0.4 Jy beam^{-1}, the integrated flux of 13.6 ± 0.6 Jy and deconvolved size of the core of $2.8'' \times 1.8''$ (P.A. $= 48°$). The flux density of 1.3 cm continuum emission is ~ 5 Jy (Mookerjea et al. 2007). Assuming that the 1.3 cm continuum emission is optically thin and the spectral index is 0.2, we estimate the free-free emission contribution of 7.9 Jy at 1.3 mm toward the continuum core of G34.26+0.15. The 1.3 mm continuum flux density corrected for free-free emission is 5.7 ± 0.5 Jy. As done by Qin et al. (2010), taking a mean dust grain size of 0.1 μm, grain emissivity of 2×10^{-5} at 1.3 mm and a dust temperature of 250 K for G34.26+0.15, we derived the H_2 gas mass and column density of $182 \pm 16\ M_{\odot}$ and $6.4 \pm 0.6 \times 10^{24}$ cm^{-2}.

3.2 Molecular Lines

The double sideband spectral mode of the SMA observations covers a bandwidth of 8 GHz.

Figure 2 only shows the SMA spectrum in which the 2 GHz spectrum is at the continuum peak position. One can see that many molecular transitions populate there. The identified species include complex oxygen-bearing molecules, nitrogen-bearing molecules and other molecules. Complex organic molecules of CH_3OH, CH_3OCHO, C_2H_5CN and HC_3N v7 $= 1$ have strong emissions. In this paper, we are only interested in the organic molecules of CH_3OH, CH_3OCH_3, CH_3OCHO, C_2H_5OH, C_2H_3CN, C_2H_5CN, CH_3CN and CH_3CCH, since more than three transitions of each of these molecules are observed, which span a wide energy range and enable us to derive physical parameters accurately. Molecular line parameters are obtained from Gaussian fitting to each transition and are presented in Table 1.

3.3 Gas Distribution

The spatial gas distributions of specific molecules are important for study of the related chemistry, since these distributions indicate the formation routes of specific molecules. The sample images of oxygen-bearing molecules and nitrogen-bearing molecules are shown in Figure 3.

According to Figure 3, there are spatial separations between oxygen-bearing and nitrogen-bearing molecules in G34.26+01.5, and peak positions of nitrogen-bearing molecules coincide with the peaks in continuum emission. The peaks of oxygen-bearing molecules move to the northeast of the continuum emission. The spatial separation of nitrogen- and oxygen-bearing molecules is also observed in G19.61–0.23, Orion KL and the W3(OH) complex (e.g., Blake et al. 1987; Qin et al. 2010, 2015).

4 DATA ANALYSIS

As seen in Table 1, multiple transitions of CH_3OH, CH_3OCH_3, CH_3OCHO, C_2H_5OH, C_2H_3CN, C_2H_5CN, CH_3CN and CH_3CCH are observed, spanning a wide energy range. Following the method used by Qin et al. (2010), we apply the rotational temperature diagram (RTD) method to calculate physical parameters of these molecules. One can use an RTD to derive rotational temperature and column density of a specific species in case multiple transitions, spanning a wide energy range, are observed (Goldsmith & Langer 1999). The energy level population of molecular transitions can be described by a single rotational temperature, if local thermodynamic equilibrium (LTE) holds and the molecular gas is optically thin.

Figure 4 presents RTDs of the observed molecules. The linear least-squares fittings to the data are made for molecules that are observed in this work. The derived rotational temperatures and column densities of the studied molecules are presented in Table 2. The fractional abundances of specific molecules relative to H_2 are derived by use of the ratio of molecular column densities to the H_2 column density. The results presented in Table 2 show that complex organic oxygen-containing molecules CH_3OH, CH_3OCH_3, CH_3OCHO and C_2H_5OH have high fractional abundances relative to H_2 of $0.06 - 1.4 \times 10^{-7}$, with gas temperatures < 200 K. The nitrogen-containing molecules (C_2H_3CN, C_2H_5CN, and CH_3CN) have high temperatures of > 290 K and low fractional abundances ranging from 1.14×10^{-10} to 1.2×10^{-18}. The situation is similar in the massive star forming regions Orion KL, G19.61–0.23 and W3(OH) in that the oxygen-containing molecules have higher fractional abundances but lower gas temperatures. Higher gas temperatures and lower fractional abundances are derived towards nitrogen-bearing molecules (Blake et al. 1987; Qin et al. 2010, 2015). In addition, CH_3CCH has an abundance of $\sim 4.8 \times 10^{-9}$ and a lower rotational temperature of 63 K. Note that single dish observations of C_2H_3CN, C_2H_5CN, CH_3OCH_3 and CH_3OCHO (Fontani et al. 2007) gave lower gas temperatures when compared to our results, and probably single dish observations contained cold gas components which provided averaged gas temperatures.

5 DISCUSSION AND CONCLUSIONS

Multiple transitions spanning a wide energy range are observed toward G34.16–0.25, which enable us to accurately derive physical parameters of gas temperature and column density. The peak offsets of oxygen- and nitrogen-containing molecules with respect to the peak position of the continuum source were observed toward G34.26+0.15 (see Fig. 3). The calculations have shown that the oxygen-containing and nitrogen-containing molecules have different molecular abundances and rotational temperatures. The

Table 1 Line Parameters

Molecule	Frequency (MHz)	Transition	$S_{ij}\mu^2$ (debye^2)	E_U (K)	I (Jy beam^{-1})	ΔV (km s^{-1})
CH_3OH	229589.073	$15_{(4,11)}-16_{(3,13)}$	4.59198	374.43849	13.2± 0.1	7.2± 0.1
	239731.344	$5_{(1,5)}-4_{(1,4)}$	3.88508	49.05924	15.1± 0.1	8.1± 0.1
	240241.502	$5_{(3,2)}-6_{(2,4)}$	0.98197	82.5315	11.8± 0.1	6.3± 0.1
	240740.621	$26_{(3,23)}-26_{(2,24)}$	26.79785	863.97661	4.4± 0.1	5± 0.1
	241042.683	$22_{(-6,16)}-23_{(-5,18)}$	6.39588	775.56583	2.3± 0.1	4± 0.1
	239397.838	$16_{(-3,14)}-17_{(0,17)}$	0.14009	378.27451	2.2± 0.1	3.5± 0.1
	227094.601	$21_{(1,20)}-21_{(0,21)}$	11.59311	557.07117	8.9± 0.1	6.2± 0.1
CH_3OCH_3	227648.12	$26_{(5,21)}$–$26_{(4,22)}$ EA	84.89383	355.76623	3.1± 0.1	5.9± 0.1
	227657.0248	$24_{(3,22)}$–$24_{(2,23)}$ EE	210.14176	285.56309	3.3± 0.1	8.8± 0.2
	226346.0514	$14_{(1,13)}$–$13_{(2,12)}$ AA	42.91412	98.86426	5.4± 0.1	6.1± 0.1
	226495.4549	$22_{(1,21)}$–$22_{(0,22)}$EE	107.91955	232.58339	2.1± 0.1	8.9± 0.2
	239326.2099	$23_{(1,22)}$–$23_{(0,23)}$ EE	107.96363	253.09072	2.2± 0.1	10.6± 0.2
	238958.2129	$32_{(1,31)}$–$32_{(4,28)}$ AA	126.48193	501.84005	1.8± 0.1	5.6± 0.2
	238016.1043	$27_{(2,25)}$–$27_{(3,25)}$ EE	218.16053	354.96978	1.8± 0.1	6.3± 0.2
	240985.0778	$5_{(3,3)}-4_{(2,2)}$ EE	54.77959	26.30846	4.1± 0.1	7.8± 0.1
	228424.4096	$26_{(3,24)}$–$25_{(4,21)}$ AA	29.05868	331.64699	0.8± 0.1	4.3± 0.4
CH_3OCHO	228211.291	$18_{(3,15)}$–$17_{(3,14)}$ E	46.25056	297.16473	1.9± 0.1	4.4± 0.2
	228628.876	$18_{(5,13)}$–$17_{(5,12)}$ E	44.23729	118.78854	5.0± 0.1	5.3± 0.1
	228651.404	$18_{(5,13)}$–$17_{(5,12)}$ A	44.24797	118.78242	5± 0.1	5.5± 0.1
	229405.021	$18_{(3,15)}$–$17_{(3,14)}$ E	46.11741	110.73904	5.8± 0.1	6.1± 0.1
	229420.342	$18_{(3,15)}$–$17_{(3,14)}$ A	46.12064	110.73143	6.3± 0.1	5.8± 0.1
	240021.14	$19_{(3,16)}$-$18_{(3,15)}$ E	48.61567	122.25813	7.2± 0.1	7.5± 0.1
	240034.673	$19_{(3,16)}$–$18_{(3,15)}$ A	48.63142	122.2513	5.2± 0.1	8.8± 0.1
	237807.626	$19_{(6,13)}$–$18_{(6,12)}$ E	45.4611	136.79123	4.6± 0.1	5.4 ±0.1
	237829.831	$19_{(6,13)}$–$18_{(6,12)}$ A	45.55653	136.78611	4.8± 0.1	5.4± 0.1
	238156.8625	$22_{(1,22)}$–$21_{(1,21)}$ A	58.16589	133.83147	11.2± 0.1	8± 0.1
	238190.191	$7_{(6,1)}-6_{(5,2)}$ A	2.52123	40.41583	0.9± 0.1	6.7± 0.5
	238368.799	$19_{(3,16)}$–$18_{(3,15)}$ A	48.61357	308.9218	1.6± 0.1	8.9± 0.3
	225756.199	$18_{(5,13)}$–$17_{(5,12)}$ E	43.47338	305.4027	1.5± 0.1	5± 0.2
	225928.659	$6_{(6,0)}-5_{(5,1)}$ A	2.51986	36.29203	2.4± 0.1	4.2± 0.1
	226435.521	$21_{(0,21)}$–$20_{(0,20)}$E	55.61866	308.8777	3.6± 0.1	6.4± 0.1
	226713.06	$20_{(2,19)}$–$19_{(2,18)}$ E	52.04002	120.22039	4.9± 0.1	7.7± 0.1
	226718.688	$20_{(2,19)}$–$19_{(2,18)}$ A	52.04707	120.20699	5.4± 0.1	7.4± 0.1
	226773.13	$20_{(1,19)}$–$19_{(1,18)}$ E	52.03546	120.21637	4.7± 0.1	7.7± 0.1
	226778.786	$20_{(1,19)}$–$19_{(1,18)}$ A	52.0425	120.20297	4.9± 0.1	9.3± 0.1
	227019.55	$19_{(2,17)}$–$18_{(2,16)}$ E	48.76106	116.573	5.5± 0.1	6.1± 0.1
	227028.121	$19_{(2,17)}$–$18_{(2,16)}$ A	48.76691	116.56277	4.6± 0.1	9.1± 0.1
	227599.261	$18_{(3,15)}$–$17_{(3,14)}$ A	46.0925	297.48196	1.5± 0.1	4.7± 0.2
C_2H_5OH	227891.911	$13_{(1,12)}$–$12_{(1,11)}$, vt= 1–1	20.6452	140.01443	2.2± 0.1	5.1± 0.2
	228886.6501	$9_{(3,6)}-9_{(2,8)}$, vt= 1–0	5.3747	110.07161	0.7± 0.1	4.8± 0.6
	229491.5539	$46_{(7,39)}$–$46_{(6,40)}$, vt= 0–0	0.24656	1020.70466	1.9± 0.1	4.7± 0.2
	240110.238	$27_{(2,25)}$–$27_{(1,26)}$	29.31314	327.23803	0.8± 0.1	4.4± 0.5
	240838.7471	$14_{(1,13)}$–$13_{(0,13)}$, vt= 0–1	9.09134	147.09916	1.6± 0.1	4.1± 0.2
	238568.1891	$6_{(1,5)}-5_{(0,5)}$, vt= 1–0	4.24277	80.72611	1.1± 0.1	5.3± 0.4
	239478.079	$14_{(2,13)}$–$13_{(2,12)}$, vt= 0–0	21.90963	148.43824	2.2± 0.1	5± 0.2
	239551.366	$14_{(2,13)}$–$13_{(2,12)}$, vt= 1–1	21.90948	153.11156	2.2± 0.1	4.9± 0.2
	225796.891	$13_{(4,9)}$–$12_{(4,8)}$, vt= 0–0	18.80219	152.09896	2± 0.1	6± 0.2
	226581.339	$26_{(2,24)}$–$26_{(1,25)}$	28.24034	304.69227	0.9± 0.1	4.2± 0.4
	227294.752	$13_{(3,10)}$–$12_{(3,9)}$, vt= 1–1	19.66545	148.56961	1.7± 0.1	5.2± 0.2
C_2H_3CN	226256.8803	$24_{(2,23)}$–$23_{(2,22)}$	1040.33362	144.79326	0.7± 0.1	5.3± 0.5
	238726.8113	$26_{(1,26)}$–$25_{(1,25)}$	1133.0669	157.37752	2.4± 0.1	4.8± 0.2
	238796.2925	$25_{(3,22)}$–$24_{(3,21)}$	1075.85721	167.9148	1.2± 0.1	6.2± 0.3
	227897.6076	$24_{(7,17)}$–$23_{(7,16)}$	958.82619	242.46929	0.7 ±0.1	7.6± 0.7
	227906.7091	$24_{(6,18)}$–$23_{(6,17)}$	982.32004	214.45704	0.9± 0.1	7.8± 0.5
	228087.2448	$24_{(11,14)}$–$23_{(11,13)}$	827.73655	396.9138	0.7± 0.1	4.3± 0.5
	228104.6144	$24_{(4,21)}$–$23_{(4,20)}$	1018.75591	171.33744	0.9± 0.1	3.9± 0.4
	228160.3049	$24_{(4,20)}$–$23_{(4,19)}$	1018.75515	171.34687	1.5± 0.1	5.6± 0.3
	229087.0477	$24_{(3,21)}$–$23_{(3,20)}$	1031.47236	156.45448	0.7± 0.1	5.7± 0.6
	229647.8388	$25_{(1,25)}$–$24_{(1,24)}$	1089.34365	145.92055	1.9± 0.1	4.7± 0.2

C_2H_5CN	227780.9718	$25_{(3,22)}$–$24_{(3,21)}$	365.32437	150.84922	3.8± 0.1	5.8± 0.1
	228483.1359	$25_{(2,23)}$–$24_{(2,22)}$	368.05881	146.59165	4.4± 0.1	5.3± 0.1
	229265.16	$26_{(2,25)}$–$25_{(2,24)}$	382.45273	154.02143	4.4± 0.1	5.3± 0.1
	240319.3368	$28_{(1,28)}$–$27_{(1,27)}$	414.0537	169.2645	5.1± 0.1	5.3± 0.1
	240429.1835	$28_{(0,28)}$–$27_{(0,27)}$	414.0245	169.24387	4.1± 0.1	5.6± 0.1
CH_3CN	2238766.0489	13_9–12_9	286.97085	658.1578	4.1± 0.1	5.8± 0.1
	238843.926	13_8–12_8	171.20193	537.03504	5± 0.1	6.5± 0.1
	238912.7154	13_7–12_7	195.68053	430.09712	8.1± 0.1	6± 0.1
	238972.3895	13_6–12_6	433.70052	337.36833	13.6± 0.1	7.1± 0.1
	239022.9241	13_5–12_5	234.7829	258.86994	13.6± 0.1	7± 0.1
	239064.2988	13_4–12_4	249.46102	194.61954	16.3± 0.1	6.7± 0.1
	239096.4966	13_3–12_3	521.81905	144.6318	17.1± 0.1	8.4± 0.1
	239119.5044	13_2–12_2	269.05112	108.91819	18.5± 0.1	6.6± 0.1
	239133.3129	13_1–12_1	273.94228	87.48682	17.7± 0.1	12.8± 0.1
CH_3CCH	239179.2812	14_4–13_4	4.81196	201.69776	1.4± 0.1	4.6± 0.2
	239211.2149	14_3–13_3	9.99811	151.14227	4.8± 0.1	5.4± 0.1
	239234.0336	14_2–13_2	5.1327	115.02278	3.4± 0.1	5.5± 0.1
	239252.2938	14_0–13_0	5.24012	86.1221	3.7± 0.1	10.7± 0.1

Table 2 Rotational Temperature, Column Density and Abundance

Molecule	Temperature (K)	Column Density (cm^{-2})	Abundance
CH_3OH	201 ± 4	$(9.1 \pm 0.4) \times 10^{17}$	$(1.4 \pm 0.1) \times 10^{-7}$
CH_3OCH_3	192 ± 40	$(4.6 \pm 1.8) \times 10^{17}$	$(7.2 \pm 3.9) \times 10^{-8}$
CH_3OCHO	190 ± 81	$(1.2 \pm 0.9) \times 10^{17}$	$(1.9 \pm 1.4) \times 10^{-8}$
C_2H_5OH	102 ± 5	$(3.6 \pm 0.4) \times 10^{16}$	$(5.6 \pm 0.6) \times 10^{-9}$
CH_3CCH	63 ± 9	$(3.1 \pm 1.1) \times 10^{16}$	$(4.8 \pm 1.7) \times 10^{-9}$
C_2H_3CN	290 ± 137	$(7.3 \pm 5.6) \times 10^{14}$	$(1.1 \pm 0.9) \times 10^{-10}$
C_2H_5CN	300 ± 130	$(8.1 \pm 6.5) \times 10^{15}$	$(1.3 \pm 1) \times 10^{-9}$
CH_3CN	298 ± 8	$(7.9 \pm 0.4) \times 10^{15}$	$(1.3 \pm 0.1) \times 10^{-9}$

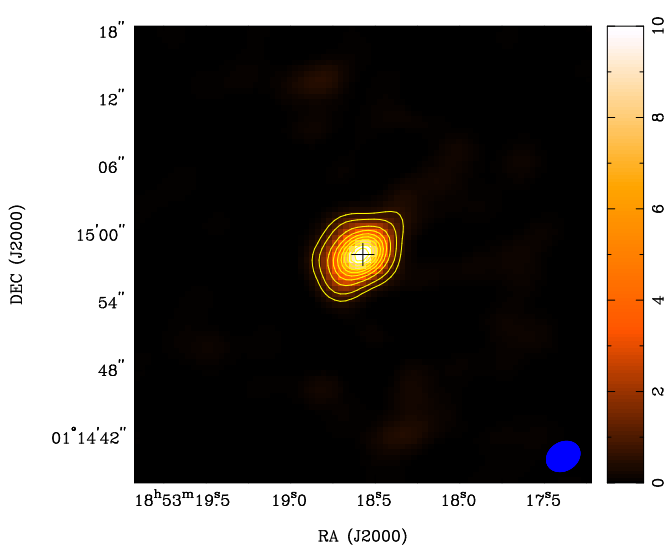

Fig. 1 1.3 mm continuum image of G34.26+0.15, with both a color scale and contours. The contours are 5%, 10%, 20%, 30%, 40%, 50%, 60%, 70%, 80%, 90% and 100% of the peak value. The plus sign indicates the peak position of the continuum.

spatial distributions, gas temperatures and fractional abundances imply there are physical and chemical differences among various species. We discuss the chemical origin of the observed molecules in the following:

CH_3OH has the highest fractional abundance of 1.4×10^{-7} when compared with other organic molecules in our observations. Higher CH_3OH abundance is also observed in the massive star-forming regions W51N, G19.61 and W3(OH) (Rong et al. 2016; Qin et al. 2010,

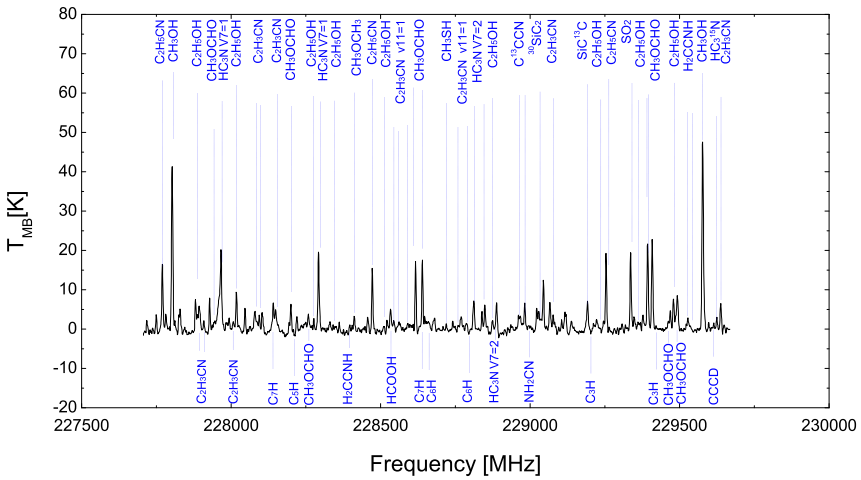

Fig. 2 Sample spectrum at the continuum peak position.

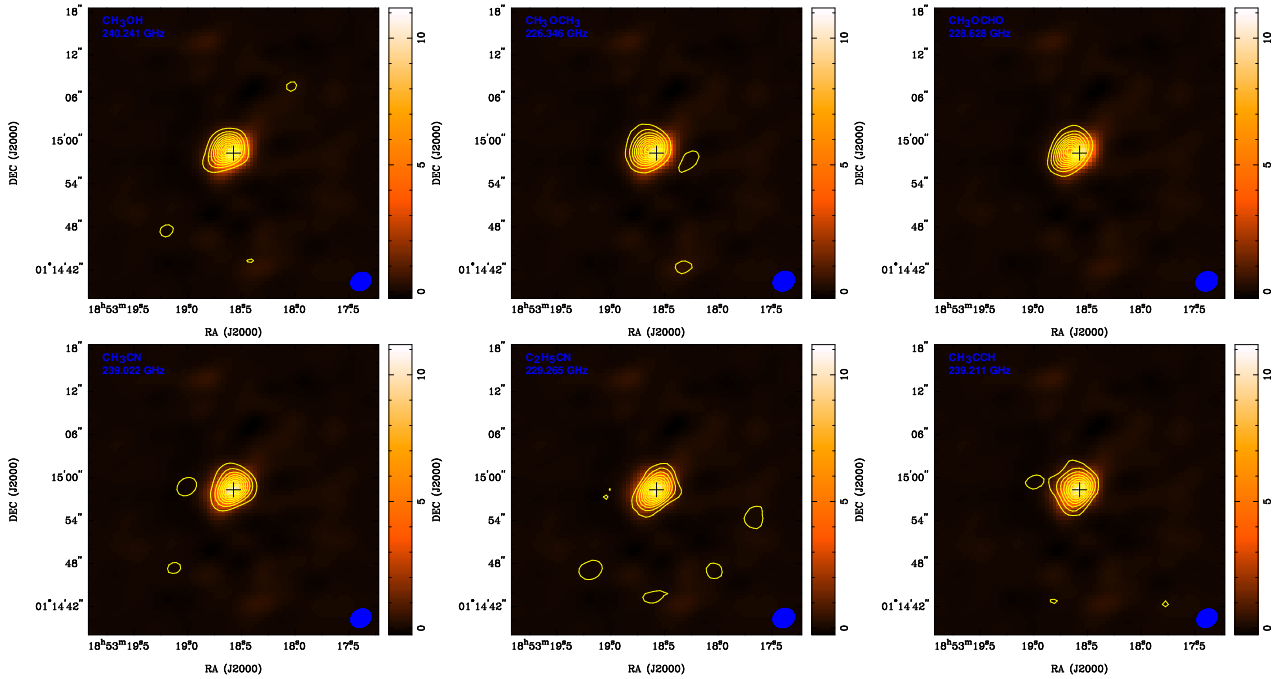

Fig. 3 Sample images of specific species overlaid on the continuum image with a color scale. The contour levels range from 10% to 90% of the maximum integrated intensity for each molecule. In each panel, the plus symbol indicates the continuum peak position. The resultant beam is displayed in the lower-right corner.

2015). The pure gas-phase chemical model cannot explain observed higher CH_3OH abundance. Grain-surface chemistry may be responsible for this complex species observed in this study. The grain chemistry suggested that C_2H_5OH may be synthesized on the grain surface through hydrogenation of CH_3CO (Charnley et al. 2004; Ohishi et al. 1995). Charnley et al. (1992) proposed that gas-phase chemistry through molecule-ion reaction of CH_3OH^+ with CH_3OH and H_2CO can produce CH_3OCH_3 and CH_3OCHO. Higher rotational temperatures but lower abundances were observed toward all nitrogen-bearing molecules when compared to oxygen-containing molecules in this observation. CH_3CN may be formed via high temperature gas phase reactions at a temperature of $\sim$ 300 K through NH_3 injection (Qin et al. 2008). C_2H_3CN and C_2H_5CN have a similar temperature of $\sim$ 300 K, while C_2H_5CN has a higher column density than C_2H_5CN. Similar gas temperatures and spatial distri-

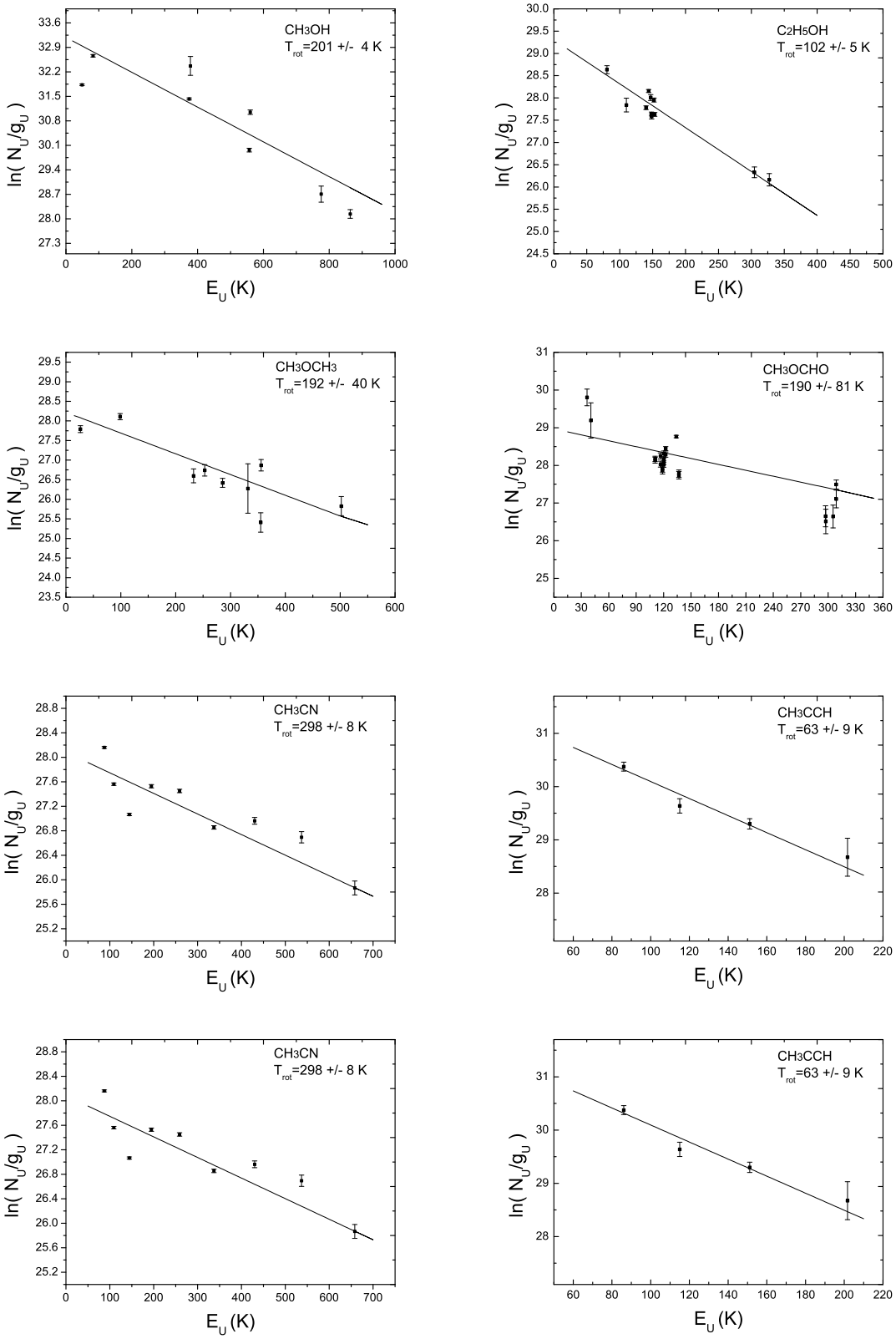

Fig. 4 RTDs. The linear least-squares fittings to the observed transitions are shown as straight lines. The filled symbols represent the observed transitions and 3σ errors are indicated by vertical bars.

butions of CH_3CN, C_2H_5CN and C_2H_3CN indicate that these nitrogen-containing species may have similar chemical originations and be formed in high temperature gas-phase reactions. CH_3OH and CH_3CN are representative oxygen- and nitrogen-containing molecules and the abundance ratio of CH_3OH to CH_3CN, 115±8, is appropriate. This value is roughly consistent with that in the UC HII region source W3(OH) (∼138) and larger than that in high mass protostar W3(H_2O) (∼16) (see Qin et al. 2015) and other high-mass young stellar objects (Bisschop et al. 2007; Gibb et al. 2000). The larger CH_3OH to CH_3CN abundance ratio in G34.26+0.15 may imply that the surrounding gas can be effectively heated by the UC HII region and then CH_3OH is evaporated from the grain surface as the cloud warms up. The derived CH_3CCH abundance of 4.8×10^{-9} is in good agreement with that in other high mass star-forming regions and larger than that in cold cores (Miettinen et al. 2006). CH_3CCH can be formed on dust grains through the reaction between CH and C_2H_4 (Canosa et al. 1997). CH_3CCH peaks at the same position as the nitrogen-bearing molecules and has lower gas temperature, which may indicate that CH_3CCH and nitrogen-bearing molecules are synthesized on the same site but are distributed in different layers of the cloud as temperature increases.

In summary, the SMA observations showed that there is a spatial separation between nitrogen- and oxygen-containing molecules. The nitrogen-bearing molecules have higher rotational temperatures but lower molecular abundances compared to the oxygen-containing species. These two groups of molecules have different chemical originations.

Acknowledgements We thank the staff at SMA for acquiring the observations. This work was partly funded by the Specialized Research Fund for the Program of Langfang Teachers University, China (LSLZ 201401), and the Natural Science Foundation of Hebei Province, China (B2014408013).

References

Avalos, M., Lizano, S., Rodríguez, L. F., Franco-Hernández, R., & Moran, J. M. 2006, ApJ, 641, 406

Bisschop, S. E., Jørgensen, J. K., van Dishoeck, E. F., & de Wachter, E. B. M. 2007, A&A, 465, 913

Blake, G. A., Sutton, E. C., Masson, C. R., & Phillips, T. G. 1987, ApJ, 315, 621

Canosa, A., Sims, I. R., Travers, D., Smith, I. W. M., & Rowe, B. R. 1997, A&A, 323, 644

Charnley, S. B., Tielens, A. G. G. M., & Millar, T. J. 1992, ApJ, 399, L71

Charnley, S. B., Ehrenfreund, P., Millar, T. J., et al. 2004, MNRAS, 347, 157

Churchwell, E. 2002, ARA&A, 40, 27

Fontani, F., Pascucci, I., Caselli, P., et al. 2007, A&A, 470, 639

Gibb, E., Nummelin, A., Irvine, W. M., Whittet, D. C. B., & Bergman, P. 2000, ApJ, 545, 309

Goldsmith, P. F., & Langer, W. D. 1999, ApJ, 517, 209

Hatchell, J., Thompson, M. A., Millar, T. J., & MacDonald, G. H. 1998, A&AS, 133, 29

Kuchar, T. A., & Bania, T. M. 1994, ApJ, 436, 117

Kurtz, S., Cesaroni, R., Churchwell, E., Hofner, P., & Walmsley, C. M. 2000, Protostars and Planets IV, eds. V. Mannings, A. Boss, & S. Russell (Tucson: Univ. Arizona Press), 299

Liu, T., Wu, Y., & Zhang, H. 2013, ApJ, 776, 29

Miettinen, O., Harju, J., Haikala, L. K., & Pomrén, C. 2006, A&A, 460, 721

Mookerjea, B., Casper, E., Mundy, L. G., & Looney, L. W. 2007, ApJ, 659, 447

Ohishi, M., Ishikawa, S.-I., Yamamoto, S., Saito, S., & Amano, T. 1995, ApJ, 446, L43

Qin, S.-L., Huang, M., Wu, Y., Xue, R., & Chen, S. 2008, ApJ, 686, L21

Qin, S.-L., Wu, Y., Huang, M., et al. 2010, ApJ, 711, 399

Qin, S.-L., Schilke, P., Wu, J., et al. 2015, ApJ, 803, 39

Rong, J., Qin, S.-L., Zapata, L. A., et al. 2016, MNRAS, 455, 1428

Wood, D. O. S., & Churchwell, E. 1989, ApJS, 69, 831